

RSC Advances



This is an *Accepted Manuscript*, which has been through the Royal Society of Chemistry peer review process and has been accepted for publication.

Accepted Manuscripts are published online shortly after acceptance, before technical editing, formatting and proof reading. Using this free service, authors can make their results available to the community, in citable form, before we publish the edited article. This *Accepted Manuscript* will be replaced by the edited, formatted and paginated article as soon as this is available.

You can find more information about *Accepted Manuscripts* in the [Information for Authors](#).

Please note that technical editing may introduce minor changes to the text and/or graphics, which may alter content. The journal's standard [Terms & Conditions](#) and the [Ethical guidelines](#) still apply. In no event shall the Royal Society of Chemistry be held responsible for any errors or omissions in this *Accepted Manuscript* or any consequences arising from the use of any information it contains.

Heteroarchitected Ag-Bi₂O₃-ZnO as a bifunctional nanomaterial

Subramanian Balachandran,^{a,d} Natarajan Prakash^b and Meenakshisundaram

Swaminathan^{c*}

^aDepartment of Chemistry, Annamalai University, Annamalainagar– 608 002, India

^bGraduate School of Science and Technology, Shizuoka University, 3-5-1 Johoku, Naka-ku, Hamamatsu 432-8011, Japan

^cNanomaterials Laboratory, International Research Centre, Kalasalingam University, Krishnankoil- 626126, Tamil Nadu, India

^dBeijing National Laboratory for Molecular Sciences, Key Laboratory of Engineering Plastics, Institute of Chemistry, Chinese Academy of Sciences, Zhongguancun North First Street 2, Beijing 100190, P. R. China

*Corresponding author. Tel./fax: +91-4144-220572.

E-mail address: chemres50@gmail.com (M. Swaminathan)

Heteroarchitected Ag-Bi₂O₃-ZnO was synthesized through simple, cost effective, template free photodeposition-hydrothermal method. This composite material represents a prospective new class of novel catalysts wherein the improved light absorption behavior of a metal doped coupled oxide, Ag-Bi₂O₃-ZnO is anticipated to enhance with the observed benefits of coupled system of Bi₂O₃-ZnO. Characterization of Ag-Bi₂O₃-ZnO revealed interesting optical and morphological characteristics. XRD patterns indicated that well-crystallized α -Bi₂O₃ was formed on the hexagonal wurtzite phase of ZnO along with Ag in the process. The HR-SEM images revealed the formation of organized intercrossed sheets and peanut shell like structure, which were composed of nanosheets and nanoparticles respectively. Elemental color mapping confirms the homogeneity of Zn, O, Ag and Bi in the catalyst. Ag-Bi₂O₃-ZnO has enhanced absorption in the UV and visible region when compared to Bi₂O₃ and ZnO. This catalyst exhibited enhanced photocatalytic activity for the degradation of Acid Red 1 (AR 1), Evens Blue (EB) and Acid Violet 7 (AV 7) under natural sun light far exceeding those of the Bi₂O₃, Ag-ZnO, Ag-Bi₂O₃ and ZnO systems at neutral pH. Ag-Bi₂O₃-ZnO was found to be stable and reusable without appreciable loss of photocatalytic activity up to five runs. Ag-Bi₂O₃-ZnO shows enhanced electrochemical methanol oxidation when compared to Ag-Bi₂O₃, Bi₂O₃-ZnO, Ag-ZnO and ZnO. Enhancement in methanol oxidation current demonstrates its high potential as anode catalyst in direct methanol fuel cells.

Introduction

The design of efficient multifunctional catalysts will be a key to the present problems of environmental pollution and energy crisis. Semiconductor oxides afford a solution to these problems. ZnO, a semiconductor photocatalyst, has fascinated intense research awareness in a broad range of applications, such as organic pollutants degradation, water splitting, and photovoltaic devices. ZnO was reported to be the most active semiconductor for the solar degradation of Acid Brown 14 among TiO₂, ZnO, SnO₂, ZrO₂, α -Fe₂O₃, WO₃ and CdS.¹ The optical properties of ZnO can be tuned by controlling not only the size and shape of the nanocrystals but also the type and concentration of appropriate doping atoms.²⁻⁵

Bismuth oxide (Bi₂O₃) is an important p-type semiconductor with four main crystallographic polymorphs denoted by α -, β -, γ -, and δ -Bi₂O₃. Bi₂O₃ with a band gap of 2.8 eV in the visible range has been widely used for various applications,⁶⁻¹⁰ and accounts for its ability to generate highly reactive species, such as O₂⁻• and OH• radicals from water for mineralization of pollutants.^{11, 12}

But, the single-component UV light sensitive photocatalysts for environmental purification applications can only utilize photons below a wavelength of 450 nm, which represents only part of the solar light spectrum. One effective way to induce solar light absorption of a semiconductor is to couple it with another semiconductor having appropriate band structure. A large number of binary coupled semiconductor materials such as TiO₂-SiO₂,¹³ Bi₂O₃-ZnO,¹¹ BiVO₄-ZnO,¹⁴ Pr₆O₁₁-ZnO,¹⁵ Bi₂S₃-ZnO¹⁶ had been reported with enhanced photocatalytic activity. The surface adaption of semiconductors with noble metals (Ag, Pt, Au) has fascinated considerable attention especially in heterogeneous photocatalysis. This can reduce the recombination of the photogenerated electron/hole pairs and lengthen their lifetime through

the conduction band electron trapping. Ag, as electron sinks, is well known due to the Schottky barrier at the metal-semiconductor interface.¹⁷ Nanocomposites such as TiO₂-SiO₂-Ag,¹⁸ TiO₂-Carbon-Ag,¹⁹ TiO₂-graphene-Ag,²⁰ TiO₂-AgBr-Ag,²¹ and TiO₂-Graphene-Fe₃O₄²² have been synthesized. The development of new visible light-active photocatalysts is one of the most important topics in photocatalysis research.²³

Methanol fuel cells (MFCs) are considered as significant power resource due to their low emissions and high energy efficiencies.²⁴⁻²⁸ However, the catalytic activity of high expensive of Pt and Pt-based electrocatalysts in MFCs diminish gradually due to chemisorption of carbonaceous intermediate products on these catalysts and this is the main barrier to the commercialization of direct methanol fuel cell (DMFC) technology.²⁹⁻³¹ Thus, it is necessary to explore non-Pt catalysts to reduce costs and to improve the efficiency of the fuel cells. A significant challenge in the development of DMFC technology is the need for highly active anode catalysts for the methanol oxidation reaction.

Fabrication of heterostructured materials for multiple applications without using template or catalyst in a cost effective, simple methodology is a highly challenging job for chemists and material scientists. Herein, we report the preparation of Ag-Bi₂O₃-ZnO photocatalyst using simple photodeposition-hydrothermal method. The electrocatalytic activity of the catalyst for the electro-oxidation of methanol in alkaline media has been investigated.

EXPERIMENTS

Reagents

Analar grade zinc nitrate hexahydrate, oxalic acid dihydrate, bismuth nitrate pentahydrate, silver nitrate, nitric acid, sodium hydroxide and absolute Methanol were obtained from Himedia chemicals and used as such. Acid Red 1 (molecular formula C₁₈H₁₃N₃Na₂O₈S₂ and molecular

weight: 509.42), Evens Blue (molecular formula $C_{34}H_{24}N_6Na_4O_{14}S_4$ and molecular weight: 960.8) and Acid Violet 7 (molecular formula $C_{20}H_{16}N_4Na_2O_9S_2$ and molecular weight: 566.47) from Colour Chem, Pondicherry and ZnO (surface area $5\text{ m}^2/\text{g}$, particle size $4.80\ \mu\text{m}$) from Merck chemicals were used as received. Deionized distilled water was employed throughout experiments.

Preparation of Ag-Bi₂O₃-ZnO

0.97 g Bi(NO₃)₃·5H₂O was dissolved in 10 mL 1.12 M nitric acid to avoid hydrolyzation of Bi³⁺ ions and before making up the solution to 100 mL, its pH was adjusted to 11 by the addition of small amount of 0.2M NaOH. Then 2.0 mL of 0.1 M AgNO₃ was quickly added to the above solution. This solution was mixed with 100 mL solution of 11.90 g of Zn (NO₃)₂·6H₂O (0.4 M) in deionized water. Finally, 100 ml solution of oxalic acid dihydrate in deionized water (0.6 M) was introduced into the above solution drop wise with stirring and stirring was continued for 2 h to ensure complete precipitation of zinc oxalate and bismuth oxalate. The resulting suspension was stirred for 1.0 h and then UV irradiation was carried out using four parallel medium pressure mercury lamps emitting 365 nm wavelength for 3 h. The reaction mixture was transferred to the Teflon lined stainless steel autoclave for the hydrothermal treatment at 120 °C for 12 h. During the process the pressure was maintained at 18 psi. The final products were filtered, washed with deionized water and ethanol several times, and dried at 80 °C for 12 h in an oven. The mixed precipitate was calcined in air at 450 °C for 12 h, to get Ag-Bi₂O₃-ZnO. The preparation process is given in scheme 1. This catalyst contains 9% Ag, 11.8% Bi₂O₃ and 80.2% ZnO. Catalysts with different percentages of Ag were prepared by a similar procedure with appropriate amount of AgNO₃ solution.

Characterization

X-ray diffraction (XRD) patterns were recorded with a Siemens D5005 diffractometer using Cu K α ($\lambda=0.151\ 418\ \text{nm}$) radiation. Maximum peak positions were compared with the standard files to identify the crystalline phase. The surface morphology of the Ag-Bi₂O₃-ZnO was studied using a field emission scanning electron microscope (FE-SEM) (Model ULTRA-55). EDS analysis was performed on gold coated samples with FE-SEM (Model ULTRA-55). HR-TEM images were taken from 200 kV Ultra High Resolution Transmission Electron Microscope (JEOL-2010) having high resolution optical microscope (Leica microscope). Diffuse reflectance spectra were recorded with Shimadzu UV-2450. Photoluminescence spectra of the samples were recorded on a Perkin Elmer LS 55 fluorescence spectrometer. The excitation wavelength used to record PL was 320 nm. UV absorbance measurements were taken using Hitachi-U-2001 spectrometer.

Photocatalytic experiments

All photocatalytic experiments were carried out under similar conditions on sunny days of April–May 2013 between 11 am and 2 pm. An open borosilicate glass tube of 50 mL capacity, 40 cm height and 20 mm diameter was used as the reaction vessel. 50 mL of dye solution ($5 \times 10^{-4}\ \text{M}$) with 200 mg of Ag-Bi₂O₃-ZnO was magnetically stirred in the dark for 30 min to attain adsorption–desorption equilibrium between the dye and Ag-Bi₂O₃-ZnO. After dark adsorption the first sample was taken. Solar irradiation was carried out in the open-air condition. The suspension was continuously aerated (airflow rate = $8.1\ \text{mL s}^{-1}$) by a pump to provide oxygen and for the complete mixing of reaction solution. During the illumination time no volatility of the solvent was observed. At specific time intervals, 2 mL of the sample was withdrawn and

centrifuged to separate the catalyst. 1 mL of the centrifugate was diluted to 10 mL and its absorbance was measured at 306, 314 and 285 nm for AR 1, EB and AV 7 dyes respectively. The absorbance at 306, 314 and 285 nm represent the aromatic content of AR 1, EB and AV 7 respectively and its decrease indicates extent of dye degradation. Solar light intensity was measured for every 30 min and the average light intensity over the duration of each experiment was calculated. The sensor was always set in the position of maximum intensity. The intensity of solar light was measured using LT Lutron LX-10/A Digital Lux meter and the intensity was $1250 \times 100 \pm 100$ lux. The intensity was nearly constant during the experiments.

Electrochemical studies

Cyclic voltammetry (CV) was performed with a CHI660 electrochemical workstation (CH Instruments, USA). Cyclic voltammetry was carried out with three electrodes, Ag/AgCl electrode as the reference electrode, a counter electrode (Platinum wire) and unmodified or modified glassy carbon electrode (GCE) as the working electrode. GCEs were polished before the experiments in sequence with 1, 0.30 and 0.05 micron aluminium/water slurry on micro cloth pads, followed by careful cleaning in 1:1 HNO₃-H₂O (v/v), ethanol, and water via ultrasonication. The working electrode was prepared by spraying the catalysts dispersed in isopropyl alcohol. Cyclic voltammograms were obtained between +1.0 and -0.1 V at a scan rate of 50 mVs⁻¹. All potentials are reported with respect to the reversible hydrogen electrode. The CO stripping voltammetry curves were obtained after adsorption of CO on catalysts at -0.2 V. To observe methanol electro-oxidation, 0.5 M methanol solution in 0.5 M NaOH was used.

Results and discussion

Preliminary study on the degradation of three azo dyes AR 1, EB and AV 7 with different wt % of Ag in Ag-Bi₂O₃-ZnO catalysts was carried out. The percentages of AR1 degradation with 3, 6, 9, 12 and 15% of Ag were found to be 67, 70, 75, 72 and 69% respectively for 60 minutes irradiation and the percentage of error is +1, or -1 in the consecutive measurements. The maximum efficiency was observed with 9 wt% Ag loaded catalyst. Similar results were obtained with EB and AV 7 degradation. Hence this 9 wt% Ag loaded Bi₂O₃-ZnO was characterized and used for further experiments. Fig. 1 (a), (b), (c) and (d), show the typical X-ray diffraction pattern of the prepared ZnO, 3wt%, 6wt%, 9wt% of Ag in Bi₂O₃-ZnO nanocatalysts respectively. The 2 θ values of prepared ZnO at 31.77, 34.49, 36.24, 56.60, 62.85, 66.38, 67.94, 69.08, 72.50 and 76.93 correspond to (1 0 0), (0 0 2), (1 0 1), (1 1 0), (1 0 3), (2 2 0), (1 1 2), (2 0 1), (0 0 4) and (2 0 2) planes of wurtzite ZnO (Fig. 1a). The hexagonal wurtzite structure of ZnO consists of alternating planes of tetrahedrally coordinated oxygen and zinc atoms arranged along the c-axis. This anisotropy results in the spontaneous polarization of certain planes, e.g., {001} or {101}, whereas other planes are nonpolar, e.g., {100}.³¹ The new peaks observed at 27.9, 30.11, 33.7, 46.6, 47.1 correspond to (121), (012), (-122), (041), (-104) planes of α -Bi₂O₃ (JCPDS # 71-2274)³² in Bi₂O₃-ZnO nanocatalysts (Fig. 1b, c and d). The crystallographic phase of the prepared Ag-Bi₂O₃-ZnO is confirmed as monoclinic α -Bi₂O₃ form present in hexagonal wurtzite ZnO base material. The relatively high intensity of the (101) peak is indicative of anisotropic growth and implies a preferred orientation of the crystallites. The peaks at 2 θ =38.2 and 46.23° correspond to (111) and (200) planes of face-centered-cubic (fcc) lattice of metallic Ag (JCPDS file no. 04-0783).³³ The increase in the concentration of Ag from 3wt% to 9wt% in Ag-Bi₂O₃-ZnO increases the intensity of Ag peaks at 2 θ =38.2 and 46.23°.

The Field emission scanning electron microscope (FE-SEM) images of 9 wt% Ag-Bi₂O₃-ZnO at three different magnifications are shown in Fig. 2. FE-SEM images show that Ag-Bi₂O₃-ZnO has an ordered mixture of heterostructured intercrossed micro sheets and nano particles (Fig. 2a-c) and the size of the particles are in the range of 20-35 nm (Fig. 2c). The nanoparticles are highlighted in fig. 2a by green circle. The hydrothermal method reported here is a simple process without rigorous conditions and hence it is a low-cost and convenient method to prepare nano sheet shaped Ag-Bi₂O₃-ZnO.

The surface morphology was further investigated by HR-SEM images (Fig. 3a-c). These images confirm that Ag-Bi₂O₃-ZnO is composed of nanoparticles and nanosheets. During the hydrothermal process nanoparticles are self-assembled to form a sheet like structures (Fig. 3). Nanosheets are attached with other nanosheets and give an intercrossed sheet like structure (Fig. 3c). This heterostructure having a large number of cavities on surfaces may enhance the dye adsorption on Ag-Bi₂O₃-ZnO and favor for active dye degradation.

To confirm the distribution of Zn, O, Bi and Ag in the catalyst, elemental mapping of FE-SEM was carried out. Fig. 4a, b, c and d show the elemental mapping for zinc, oxygen, bismuth and silver respectively. It is evident from the Fig.4a and b that Zn and O are higher in density. There is a homogenous distribution of Bi and Ag at lower concentration (Fig. 4c and d). Thus elemental mapping shows that the catalyst is composed of Zn, O, Bi and Ag. This also indicates the purity of the catalyst Ag-Bi₂O₃-ZnO.

Typical TEM images of the Ag-Bi₂O₃-ZnO are shown in Fig. 5a-c. This exhibits assembled nanoparticles with a large number of sheets. TEM images show a sheet with sphere like structure of irregular morphology. Fig. 5d shows the high-resolution TEM image of the

Ag-Bi₂O₃-ZnO. The lattice spacing of 0.328 nm corresponds to the interlayer spacing of the (012) plane of the α -Bi₂O₃ phase and lattice spacing of 0.256 nm is for (101) planes of wurtzite ZnO.³³ The lattice fringes with 0.236 nm spacing were assigned to the Ag (111) plane. The results match exactly with XRD pattern discussed earlier.

In order to find out the presence of elements and to determine their valance states in Ag-Bi₂O₃-ZnO, XPS study was carried out. Survey spectrum in Fig. 6a shows the presence of Zn, O Bi and Ag. Carbon 1s peaks of the Ag-Bi₂O₃-ZnO are ascribed to adventitious hydrocarbon from XPS instrument itself. In Fig. 6b, the O1s profile is asymmetric and can be fitted to two symmetrical peaks α and β locating at 530.2 and 532.2 eV, respectively, indicating two different kinds of O species in the sample. The peaks α and β should be associated with the lattice oxygen (O_L) of ZnO and chemisorbed oxygen (O_H) respectively.³⁴ Fig. 6c presents the XPS spectra of Zn 2p, and the peak positions of Zn 2p_{1/2} and Zn 2p_{3/2} locate at 1045.1 eV and 1021.9 eV. Comparing the peak positions to those in the *Handbook of X-Ray Photoelectron Spectroscopy*, we can conclude that: (i) Zn is in the state of Zn²⁺ and (ii) the whole XPS spectra have a downward shift of 0.5 eV since the standard peak position of Zn 2p_{3/2} is at 1022.4 eV.³⁵ Two signals ascribed to Bi 4f_{7/2} and Bi 4f_{5/2} at binding energies of 158.6 and 164.1 eV are observed in Fig. 6d. There are two peaks locating at 368.4 and 374.5 eV, which are attributed to Ag 3d_{5/2} and Ag 3d_{3/2}, respectively (Fig. 6e). According to Zhang *et al*, these two peaks can be attributed to metallic Ag (Ag⁰).³⁶ The binding energy peaks of Ag 3d_{5/2} for the Ag/ZnO sample shifts upward when compared with the corresponding value of the synthesized pure metallic Ag (Binding Energy value of Ag⁰ is 368.2). The shift must be due to the strong interaction between Ag and ZnO.

Optical Studies: The UV – visible diffuse reflectance spectra of the Ag-Bi₂O₃-ZnO nanocomposite and ZnO were measured to determine their light absorption characteristics (Fig. 7). The wavelength distribution of the absorbed light is a significant property of photocatalysts. Ag-Bi₂O₃-ZnO nanocomposite has higher UV and visible light absorbance, as indicated by the diffuse reflectance spectrum in absorption mode (Fig.7b). The Ag-Bi₂O₃-ZnO catalyst shows the enhanced absorption in the visible region. The extended absorption of the Ag-Bi₂O₃-ZnO nanocomposite in the visible region, is due to the typical surface Plasmon band exhibited by the AgNPs.³⁷

Photoluminescence (PL) measurements were performed to determine the charge recombination efficiency of the Ag-Bi₂O₃-ZnO nanocomposite and ZnO because the photocatalytic activity is related closely to the recombination rate of photoexcited electrons and holes. Fig. 8 shows the PL spectra of the Ag-Bi₂O₃-ZnO (Fig. 8b) nanocomposite and ZnO (Fig. 8a). Both spectra mainly consist of two emission bands: a band at 416 nm (2.98 eV) and a blue-green band at 485 nm (2.56 eV). The strong UV emission at 416 nm corresponds to the electron-hole recombination.³⁸⁻⁴¹ Reduction of PL intensity at 416 nm of Ag-Bi₂O₃-ZnO when compared to prepared ZnO indicates the suppression of recombination of the photogenerated electron-hole pair. The emission intensity of the Ag-Bi₂O₃-ZnO nanocomposite is lower than that of ZnO, suggesting that the anchoring of Ag, and Bi₂O₃ quench the fluorescence from the ZnO nanoparticles and prolong the electron-hole pair lifetime enhancing the photocatalytic activity of Ag-Bi₂O₃-ZnO.

Photocatalytic Activity of the heterostructured Ag-Bi₂O₃-ZnO

Photocatalytic degradation of Acid Red 1 (AR 1) under different conditions is shown in Fig. 9. Dye is resistant to self-photolysis and for the same experiment with Ag-Bi₂O₃-ZnO in

dark, a small decrease (8%) in dye concentration was observed due to the adsorption of dye on the catalyst. AR 1 undergoes 98.6% degradation in the presence of Ag-Bi₂O₃-ZnO under natural sunlight in 90 min. But, prepared Ag-Bi₂O₃, Ag-ZnO, Bi₂O₃ and ZnO produced 74, 85, 62 and 81% degradations, respectively in 90 min. This shows that Ag-Bi₂O₃-ZnO is most efficient in AR 1 degradation than other photocatalysts (Fig. 9). Based on the results, it is obvious that the higher photocatalytic activity of Ag-Bi₂O₃-ZnO is due to the Ag and Bi₂O₃ dopants. To test the efficiency of the catalyst on the degradations of other dyes, we had carried out the experiments on the degradation of EB and AV 7 under the same conditions. The degradation of three azo dyes AR1, EB and AV 7 at different irradiation times are shown in figs. S2, S3 and S4 respectively. There is no significant change in UV-Vis spectra of dyes during irradiation, but the intensity decrease gradually during degradation. This reveals that the intermediates do not absorb at analytical wavelengths. Similar results were observed in the photocatalytic degradation of azo dyes.^{14, 15} Fig. S5 shows the percentages of degradation of EB and AV 7 along with AR1 using Ag-Bi₂O₃-ZnO at different irradiation times. All the three dyes undergo almost complete degradation in 90 min. The results reveal that this catalyst is efficient in the degradation of azo dyes. In the case of EB dye, 44% of dye was absorbed by Ag-Bi₂O₃-ZnO. Experiments were conducted to find out whether the adsorbed dye molecules had been completely degraded by the reported procedure.⁴² The results revealed that the adsorbed dye underwent complete degradation in 90 minutes.

The percentage of degradation in the solar process is affected by variables such as the pH and catalyst loading. The effects of these variables were studied using the azo dyes (AR 1, EB and AV 7) with Ag-Bi₂O₃-ZnO. The acid-base property of the metal oxide surfaces can have considerable implications on their photocatalytic activity. Percentages of degradation at different

pH from 3-11 for three azo dyes are shown in Fig.10. It is observed that the degradation rate increases with an increase in pH up to 7 and then decreases. After 90 min of irradiation, the percentages of AR 1 degradation are 53, 71, 96, 78 and 62 at pH 3, 5, 7, 9 and 11, respectively. The optimum pH is found to be 7 for AR1 degradation and a similar trend is observed for EB and AV 7 dyes. Low removal efficiency at the acidic pH range may be due to the dissolution of ZnO in Ag-Bi₂O₃-ZnO. To find out the reason for the effect of pH on degradation efficiency, zero point charge (ZPC) of the catalyst was determined by the potentiometric titration method.⁴³ Zero point charge of Ag-Bi₂O₃-ZnO is found to be 7.1, which is less than ZPC of ZnO (9). When the pH is above ZPC, the surface charge density of the catalyst becomes negative. This affects the adsorption of dye molecules, which exist as anions in the whole range of pH studied. Hence the degradation efficiency is low at pH 9 and 11.

The reusability of Ag-Bi₂O₃-ZnO was tested for the degradation of azo dyes under identical reaction conditions. After complete degradation, the catalyst was separated and washed with large amount of deionized water. The recovered catalyst was dried in hot air oven at 100 °C for 90 min and used for a second run. Fig. S6 shows the results of dyes degradation for five runs. Ag-Bi₂O₃-ZnO exhibits remarkable photostability as the AR 1 degradation percentages are 98, 96, 94.0, 94 and 94 for 90 min in the first, second, third, fourth and fifth run respectively. There is no significant change in the degradation efficiency of Ag-Bi₂O₃-ZnO after third run. After completion of degradation reaction, the solution was tested for Bi³⁺ leaching with sodium sulfide. There is no precipitation of bismuth sulfide (Black color). As there is no leaching of Bi³⁺ this catalyst is non-toxic for the wastewater treatment.

Mechanism of degradation

Mechanism of the photocatalytic activity of the Ag-Bi₂O₃-ZnO composite is proposed in scheme 2. Three main reasons for the increase in the photocatalytic efficiency of metal doped coupled oxide: (i) Visible absorbance Ag-Bi₂O₃-ZnO increased when compared to prepared ZnO, (ii) Band energy levels of Bi₂O₃ and ZnO are suitable for charge separation and (iii) Ag metal can act as electron trap. The conduction band edges of ZnO and Bi₂O₃ are situated at -0.38 and +0.32 eV, while the valence band edges of Bi₂O₃ and ZnO are at +2.78 eV and 2.84 eV respectively as shown in Scheme 2. The CB of Bi₂O₃ is much more positive (+ 0.7 eV) than ZnO whereas VB of Bi₂O₃ is slightly more negative (-0.06 eV) than ZnO. Hence there is a greater tendency for the flow of electrons from ZnO to Bi₂O₃. As there is no significant difference in VB levels, the tendency for the holes to flow in to Bi₂O₃ will be less. This makes the charge separation effective. The enhanced charge separation is also revealed by the reduction of PL intensity of the catalyst when compared to ZnO (Fig. 8). Further the separation of photogenerated electron-hole may be due to the formation of heterojunction between ZnO and Bi₂O₃, leading to enhancement of photocatalytic activity. In addition to this 'Ag' metal can trap the electron from ZnO and Bi₂O₃, inhibiting the recombination of electrons and holes in Ag-Bi₂O₃-ZnO. Holes remained on ZnO valence band and electrons concentrated on Bi₂O₃ conduction band, enabled this type of three component system with strong oxidation and reduction capabilities to generate superoxide (O₂^{•-}), and hydroxyl radicals (OH[•]) for the dye degradation.

In the case of EB dye, a dye-sensitized mechanism is also possible for the degradation. We carried out the degradation of EB with 365 nm UV light ($I_{UV} = 1.381 \times 10^{-6}$ Einstein L⁻¹ s⁻¹) under the same conditions used for natural sun light. It was found that EB underwent 76.3%

degradation with UV light, but under the same conditions 90% degradation occurred with solar light in 75 min. The higher efficiency in solar light indicates the presence of a dye-sensitized mechanism in addition to Ag-Bi₂O₃-ZnO sensitization. This occurs when more dye molecules are adsorbed on the semiconductor surface (42.6% EB adsorption in dark). Dye is sensitized by solar irradiation and loses an electron (Eqn. 1) and this electron is transferred to the conduction band of ZnO. This subsequently increases electron transfer to the adsorbed oxygen producing superoxide radicals (Eqn. 2). Dye molecules are degraded by the superoxide radicals produced by the dye sensitization mechanism (Eqn. 3). Further, to prove the dye-sensitized mechanism, we had also carried out an experiment for degradation of colorless 4-nitrophenol by Ag-Bi₂O₃-ZnO with UV and solar light. We found that degradation of colorless 4-nitrophenol (absorbing only in the UV region) was more efficient in UV light (81.9%) than in solar light (54.2%) in 75 min under the same conditions, indicating the presence of only catalyst sensitized mechanism in the degradation of 4-nitrophenol. This confirms the presence of dye-sensitized mechanism for degradation of EB dye.



Electrocatalytic Methanol Oxidation

The structure of the electrode greatly influences its electrocatalytic activity. It has been proved that the electro-oxidation of methanol is a surface-sensitive reaction.^{29, 30} Pt wire and Ag/AgCl electrodes were used as the counter and reference electrodes, respectively. Fig.11 shows the cyclic voltammograms (CVs) of glass carbon electrode coated with prepared ZnO (a),

Ag-Bi₂O₃-ZnO (b) taken in N₂ saturated 0.5 M NaOH solution at a scan rate of 50 mV s⁻¹. The CVs (a and b) show typical potential regions for hydrogen adsorption/desorption and the formation/reduction of surfaces of Metal oxide or Metal-OH_{ads} ZnO and Ag-Bi₂O₃-ZnO.

The smaller size and good dispersion of Ag-Bi₂O₃-ZnO modified GCE are favorable for the oxidation of methanol. Two peaks of methanol oxidation under anodic condition are clearly observed (Fig. 11a and b). The oxidation peak in the forward scan corresponds to the oxidation of freshly chemisorbed species coming from methanol adsorption and the reverse oxidation peak is primarily associated with removal of carbonaceous species not completely oxidized in the forward scan. The magnitude of the peak current on the forward scan indicated the electrocatalytic activity of the coated catalysts for methanol oxidation. It is clearly seen that Ag-Bi₂O₃-ZnO catalyst exhibits a current density of 3.13 mA, which is about 3 times higher than that of ZnO (1.12 mA).

It is well recognized that the stability of catalysts is essential for the application of fuel cells. However, redox reactions on the surface of catalysts often cause inactivation of catalyst. To find out the electrocatalytic stability of the catalysts under continuous operating conditions, long-term chronoamperometric experiments were carried out in 0.5 M NaOH + 0.5 M methanol solution.⁴⁴ Fig. S7 shows the curves of current densities versus time recorded at -0.1 V for 1000 s. All these catalysts initially show a rapid decrease in current for the oxidation of methanol, and then a relatively steady current is achieved. The rapid current decay showed the poisoning of the electrocatalysts, likely due to the formation of intermediate and some poisoning species during the methanol oxidation reaction.^{45,46} It is found that the current decay for the reaction on the Ag-Bi₂O₃-ZnO (curve b) is significantly less than on the prepared ZnO (curve a). This suggests that the Ag-Bi₂O₃ loading plays a critical role in promoting the methanol

oxidation, which could be attributed to the intrinsic electron transfer characteristic of Ag-Bi₂O₃-ZnO. This reveals the higher stability of the Ag-Bi₂O₃-ZnO catalyst for methanol oxidation than ZnO.

CONCLUSIONS

Heteroarchitected Ag-Bi₂O₃-ZnO semiconductor photocatalyst was synthesized by the photodeposition-hydrothermal method and characterized. The HR-SEM images revealed the formation of well-organized intercrossed sheets composed of nanosheets and nanoparticles respectively. Elemental color mapping confirms the homogeneity of Zn, O, Ag and Bi in the catalyst. Ag-Bi₂O₃-ZnO has a nanoparticles-intercrossed Sheet like morphology and with high porosity. The Ag-Bi₂O₃-ZnO has increased absorption in the UV and Visible region. Ag-Bi₂O₃-ZnO was more efficient in dye degradation than the prepared ZnO, Ag-Bi₂O₃, and TiO₂-P25 under natural sunlight. The optimum pH for the efficient removal of dye was found to be 7. This Hydrothermal route for the fabrication of Ag-Bi₂O₃-ZnO is effective, fast, convenient, and eco-friendly. A mechanism for high charge separation efficiency is proposed. This catalyst was found to stable and reusable. Electrocatalytic activity of Ag-Bi₂O₃-ZnO nanocomposite exhibited enhanced current production by methanol oxidation under room temperature.

AUTHOR INFORMATION

Corresponding Author

*E-mail: chemres50@gmail.com, m.swaminathan@klu.ac.in, . Tel./fax: +91-4144-220572.

Notes

The authors declare no competing financial interest.

ACKNOWLEDGEMENTS

We are grateful to the Council of Scientific and Industrial Research, New Delhi, for the financial support through Research Grant no. 21 (0799) /10 / EMR-II. One of the authors Dr. S. Balachandran is thankful to the UGC Networking Resource Centre, University of Hyderabad for providing characterization facility and to Dr. Tushar Jana, School of Chemistry, University of Hyderabad for the laboratory facility. Authors are grateful to Dr. P.V. Satyam, Institute of Physics, Bhubaneswar for using HR-TEM facility.

Notes and references

- 1 S. Sakthivel, B. Neppolian, M.V. Shankar, B. Arabindoo, M. Palanichamy and V. Murugesan, *Sol. Energy Mater. Sol. Cells*, 2003, **77**, 65-82.
- 2 C. G. Van de Walle, *Phys. Rev. Lett.*, 2000, **85**, 1012–1015.
- 3 K. T. Ramakrishna, H. Gopaldaswamy and P. J. Reddy, *Cryst. Growth*, 2000, **210**, 516–520.
- 4 P. Cao, D. X. Zhao, J. Y Zhang, D. Z. Shen, Y. M. Lu, B. Yao, B. H. Li, Y. Bai and X. W. Fan, *Appl. Surf. Sci.*, 2008, **254**, 2900–2904.
- 5 J. B. Yi, C. C. Lim, G. Z. Xing, H. M. Fan, L. H. Van, S. L. Huang, K. S. Yang, X. L. Huang, X. B. Qin, B. Y. Wang, T. Wu, L. Wang, H. T. Zhang, X. Y. Gao, T. Liu, A. T. S. Wee, Y. P. Feng and J. Ding, *Phys. Rev. Lett.* 2010, **104**, 137201-137204.
- 6 A. Cabot, A. Marsal, J. Arbiol and J. R. Morante, *Sens. Actuators B*, 2004, **99**, 74–89.
- 7 L. Leontie, M. Caraman, M. Delibas and G. I. Rusu, *Mater. Res. Bull.*, 2001, **36**, 1629-1637.
- 8 D. Kulkarni and I. E. Wachs, *Appl. Catal., A: Chem.*, 2002, **237**, 121–137.
- 9 J. Switzer, M. Shumsky and E. Bohannon, *Science*, 1999, **284**, 293–296.
- 10 C. E. Mohn, S. Stolen, S. T. Norberg and S. Hull, *S. Phys. Rev. Lett.*, 2009, **102**, 155502–155506.
- 11 S. Balachandran and M. Swaminathan, *J. Phys. Chem. C*, 2012, **116**, 26306–26312.
- 12 M. Muruganandham, R. Amutha, G. Juan Lee, S. Han Hsieh, J. J. Wu and M. Sillanpaa, *J. Phys. Chem. C*, 2012, **116**, 12906–12915.

- 13 D. Yang, C. Chen, Z. Zheng, H. Liu, E. R. Waclawik, Z. Yan, Y. Huang, H. Zhang, J. Zhao and H. Zhu, *Energy Environ. Sci.*, 2011, **4**, 2279–2287.
- 14 S. Balachandran, N. Prakash, K. Thirumalai, M. Muruganandham, M. Sillanpaa and M. Swaminathan, *Ind. Eng. Chem. Res.*, 2014, **53**, 8346–8356.
- 15 S. Balachandran, K. Thirumalai and M. Swaminathan, *M. RSC Adv.*, 2014, **4**, 27642–27653.
- 16 S. Balachandran and M. Swaminathan, *Dalton Trans.*, 2013, **42**, 5338–5347.
- 17 Y. Liang, H. Wang, S. H. Casalongue, Z. Chen and H. Dai, *Nano Res.*, 2010, **3**, 701–705.
- 18 C. Ren, B. Yang, M. Wu, J. Xu, Z. Fu, Y. Lv, T. Guo, Y. Zhao and C. Zhu, *J. Hazard. Mater.*, 2010, **182**, 123–129.
- 19 (a) Q. Chen, H. Shi, W. Shi, Y. Xu and D. Wu, *Catal. Sci. Technol.*, 2012, **2**, 1213–1220. (b) C. Liu, D. Yang, Y. Jiao, Y. Tian, Y. Wang, and Z. Jiang, *ACS Appl. Mater. Interfaces*, 2013, **5**, 3824–3832.
- 20 P. Zhang, C. Shao, Z. Zhang, M. Zhang, J. Mu, Z. Guo, Y. Sun and Y. Liu, *J. Mater. Chem.*, 2011, **21**, 17746–17753.
- 21 Y. Wen, H. Ding and Y. Shan, *Nanoscale*, 2011, **3**, 4411–4417.
- 22 G. Tian, Y. Chen, H. L. Bao, X. Meng, K. Pan, W. Zhou, C. Tian, J. Q. Wang and H. Fu, *J. Mater. Chem.*, 2012, **22**, 2081–2088.
- 23 Y. Lin, Z. Geng, H. Cai, L. Ma, J. Chen, J. Zeng, N. Pan and X. Wang, *Eur. J. Inorg. Chem.*, 2012, **2012**, 4439–4444.
- 24 Z. L. Liu, B. Zhao, C. L. Guo, Y. J. Sun, Y. Shi, H. B. Yang and Z. Li, *J. Colloid Interface Sci.*, 2010, **351**, 233–238.

- 25 Y. M. Li, L. H. Tang and J. H. Li, *Electrochem. Commun.*, 2009, **11**, 846–849.
- 26 R. Ganesan and J. S. Lee, *Angew. Chem., Int. Ed.*, 2005, **44**, 6557–6560.
- 27 Q. F. Yi, F. J. Niu, L. H. Song, X. P. Liu and H. D. Nie, *Electroanalysis*, 2011, **23**, 2232–2240.
- 28 Z. Liu, X. Zhang and L. Hong, *Electrochem. Commun.*, 2009, **11**, 925–928.
- 29 R. M. A. Hameed and K. M. E. Khatib, *Int. J. Hydrogen Energy*, 2010, **35**, 2517–2529.
- 30 Y. Zhang, G. Chang, S. Liu, J. Tian, L. Wang, W. Lu, X. Qin and X. Sun, *Catal. Sci. Technol.*, 2011, **1**, 1636–1640.
- 31 Z. Y. Jiang, Q. Kuang, Z. X. Xie and L. S. Zheng, *Adv. Funct. Mater.*, 2010, **20**, 3634–3645.
- 32 N. Pugazhenthiran, P. Sathishkumar, S. Murugesan and S. Anandan, *Chem. Eng. J.*, 2011, **168**, 1227–1233.
- 33 D. Lin, H. Wu, R. Zhang and W. Pan, *Chem. Mater.*, 2009, **21**, 3479–3484.
- 34 J. J. F. Moudler, W. F. Stickle, P. E. Sobol and K. D. Bomben, Perkin- Elmer Corp , Eden Prairie, MN, 1995, p. 127.
- 35 C. D. Wagner, W. M. Riggs, L. E. Davis and J. F. Moulder, Perkin Elmer, Eden Prairie, 1979, p. 81
- 36 L. Kuai, B. Geng, X. Chen, Y. Zhao and Y. Luo, *Langmuir*, 2010, **26**, 18723–18727.
- 37 Z. Zhan, J. An, H. Zhang, R. V. Hansen and L. Zheng, *L. ACS Appl. Mater. Interfaces*, 2014, **6**, 1139–1144.
- 38 V. Stikant and D. R. Clarke, *J. Appl. Phys.*, 1998, **83**, 5447–5451.

- 39 S. C. Lyu, Y. Zhang, H. Ruh, H. Lee, H. Shim, E. Suh and C. J. Lee, *J. Chem. Phys. Lett.*, 2002, **363**, 134-138.
- 40 L. Bergman, X. B. Chen, J. L. Morrison, J. Huso and A. P. Purdy, *J. Appl. Phys.*, 2004, **96**, 675-682.
- 41 J. Wang and L. Gao, *Solid State Commun.*, 2004, **132**, 269-271.
- 42 R. Velmurugan, B. Krishnakumar, B. Subash and M. Swaminathan, *M. Sol. Energy Mater. Sol. Cells*, 2013, **108**, 205-212.
- 43 S. Subramanian, J. S. Noh and J. A. Schwarz, *J. Catal.*, 1988, **114**, 433-439.
- 44 Z. Y. Zhou, Z. Z. Huang, D. J. Chen, Q. Wang, N. Tian and S. G. Sun, *S. G. Angew. Chem. Int. Ed.*, 2010, **49**, 411-414.
- 45 (a) Y. H. Qin, H. H. Yang, X. S. Zhang, P. Li and C. A. Ma, *Int. J. Hydrogen Energy*, 2010, **35**, 7667-7674; (b) R. N. Singh, A. Singh and Anindita, *Int. J. Hydrogen Energy* 2009, **34**, 2052-2057; (c) R. N. Singh, A. Singh and Anindita, *Carbon*, 2009, **47**, 271-278; (d) L. F. Dong, R. R. S. Gari, Z. Li, M. M. Craig and S. F. Hou, *Carbon*, 2010, **48**, 781-787.
- 46 Y. C. Zhao, L. Zhan, J. N. Tian, S. L. Nie and Z. Ning, *Electrochim. Acta*, 2011, **56**, 1967-1972.

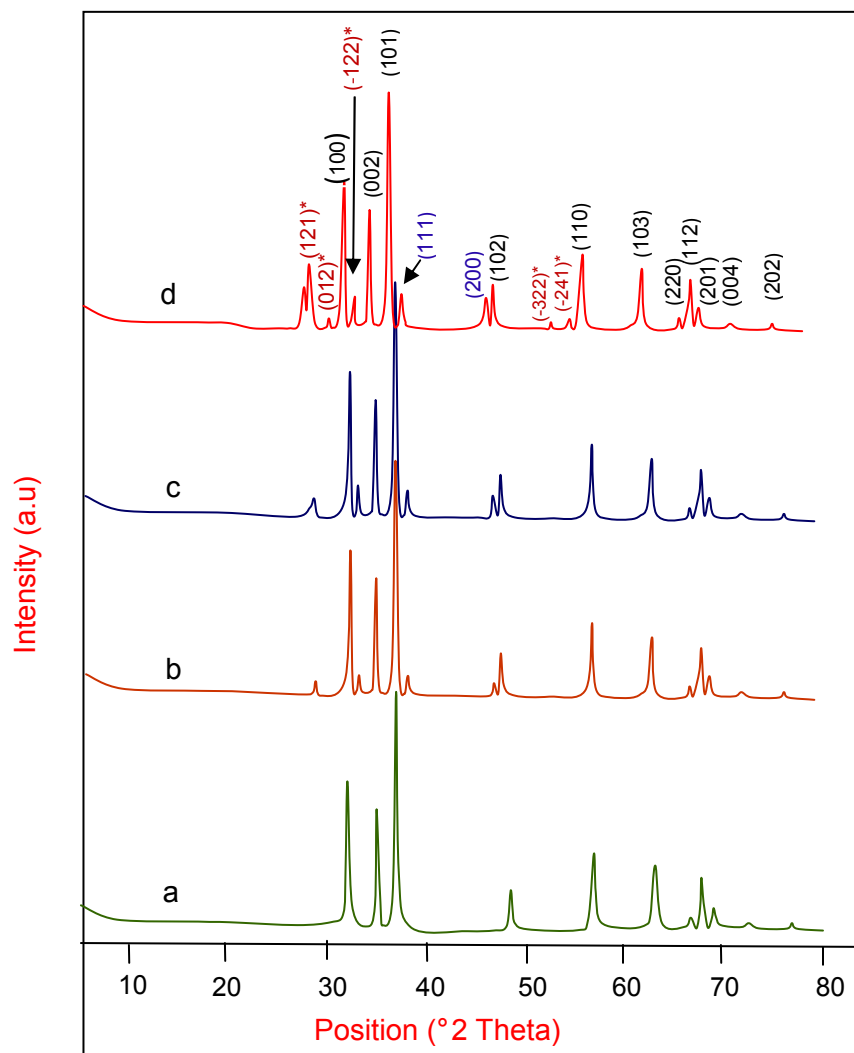


Fig. 1 XRD patterns of (a) Prepared ZnO and (b) 3wt% Ag-Bi₂O₃-ZnO, (c) 6wt% Ag-Bi₂O₃-ZnO and (d) 9wt% Ag-Bi₂O₃-ZnO.

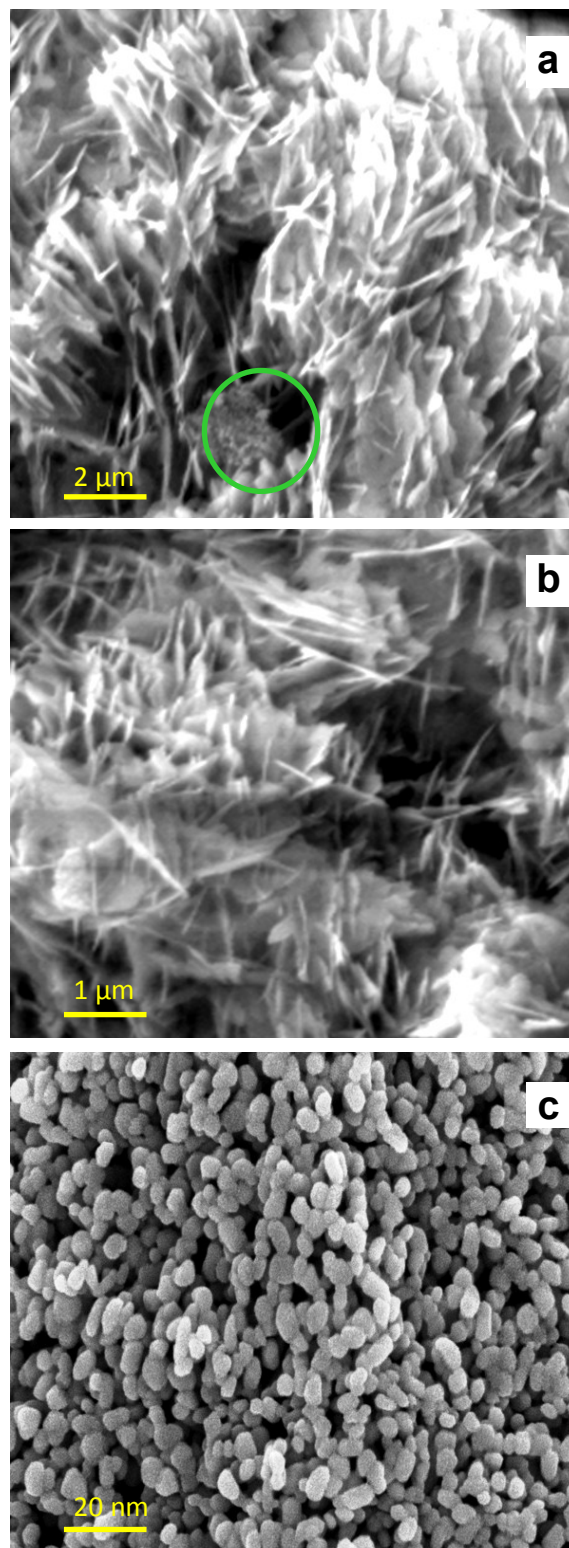


Fig. 2 FE-SEM images of 9wt% Ag-Bi₂O₃-ZnO at different magnification (a) 2 μm (nano particles are highlighted by green circle), (b) 1 μm and (c) 50 nm

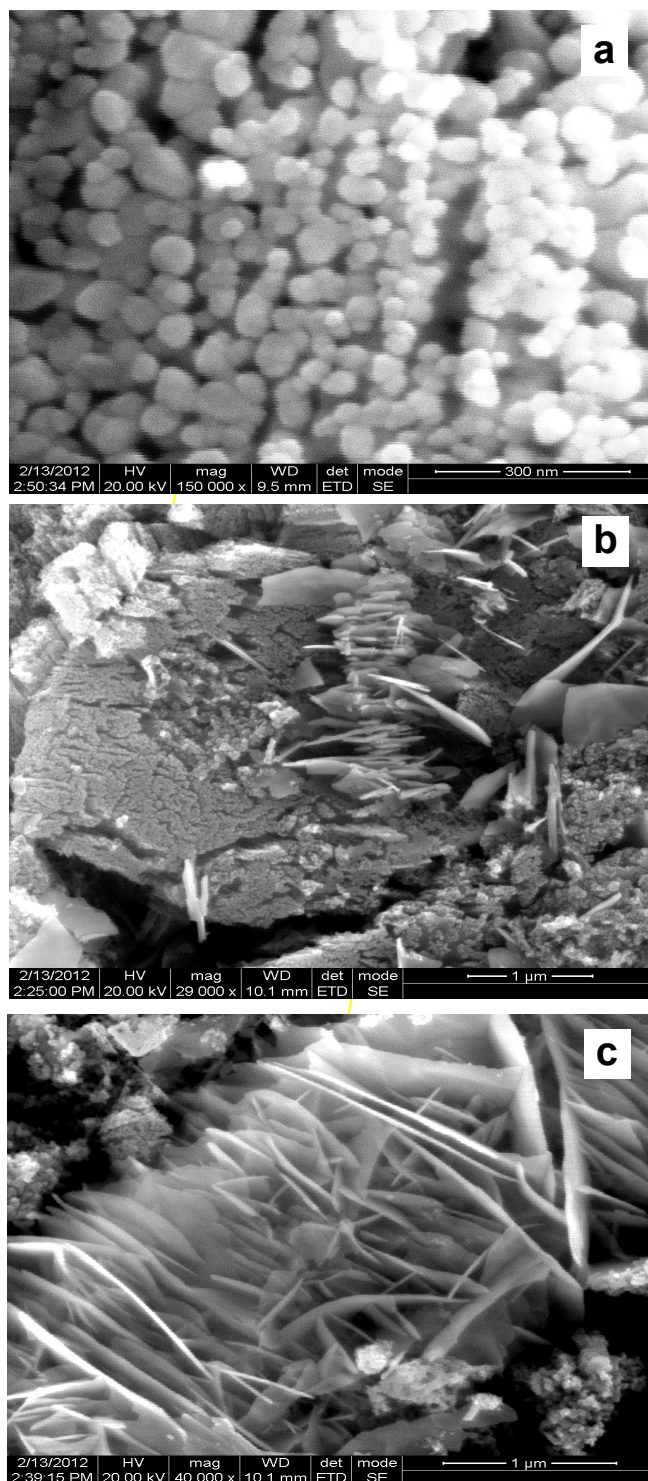


Fig. 3 HR-SEM images of 9wt% Ag-Bi₂O₃-ZnO at different magnification (a) 300 nm, (b) 1 μm and (c) 1 μm

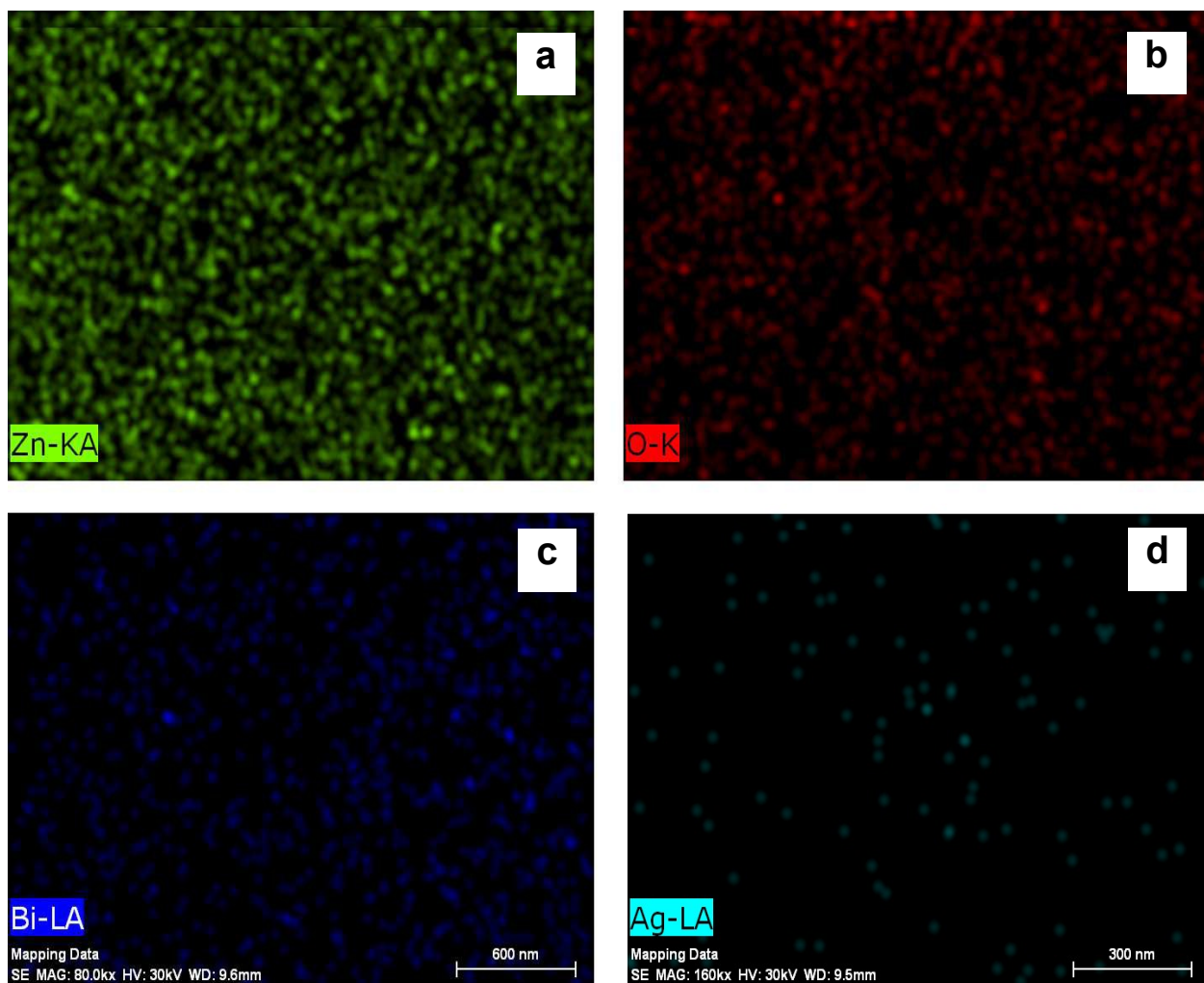


Fig. 4 FESEM elemental colour mapping of 9 wt% Ag-Bi₂O₃-ZnO (a) Zn, (b) O, (c) Bi and (d) Ag.

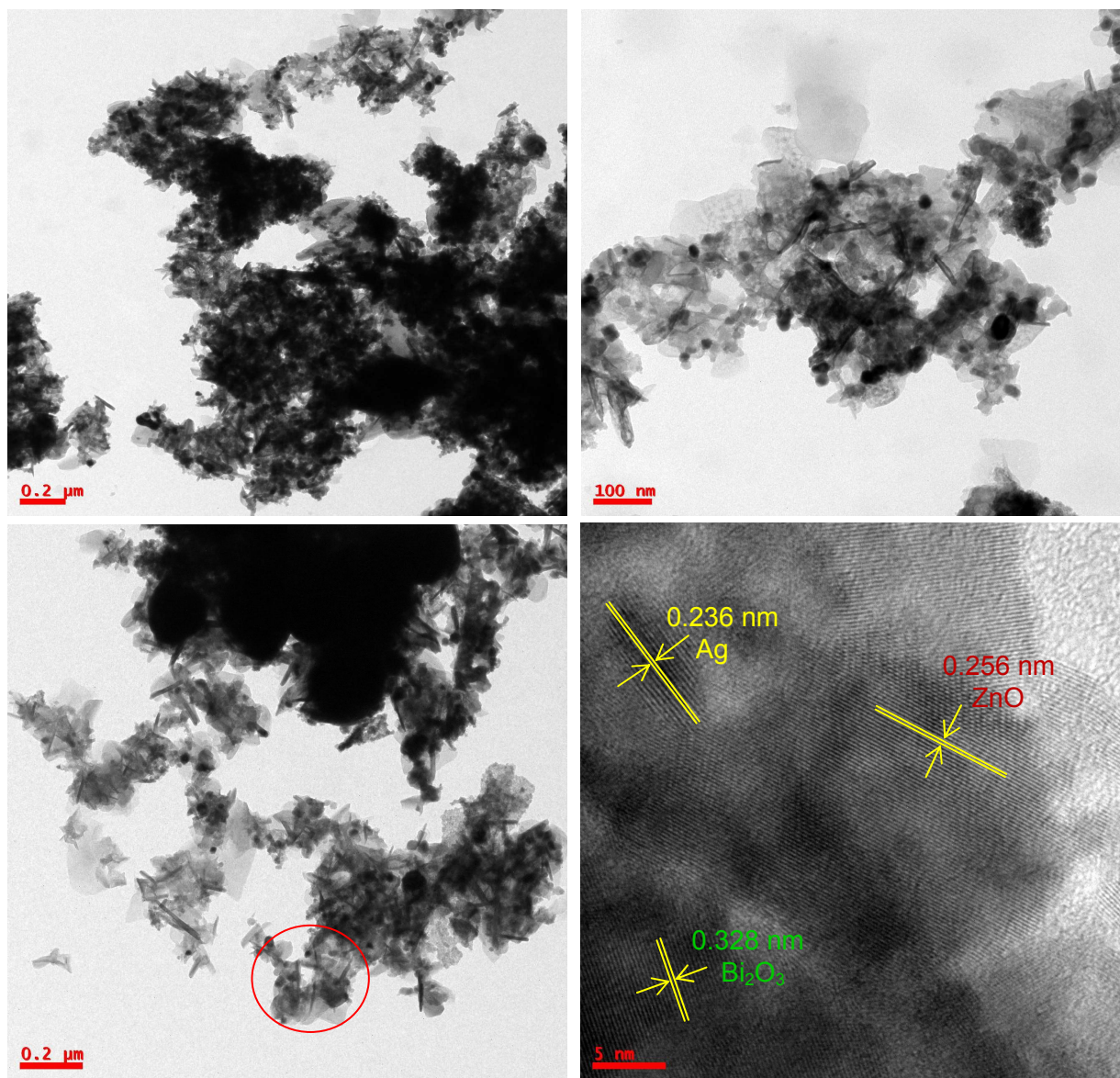


Fig. 5 TEM images of 9 wt% Ag-Bi₂O₃-ZnO (a), (b), (c) particle distribution and (d) HR-TEM image (lattice fringes)

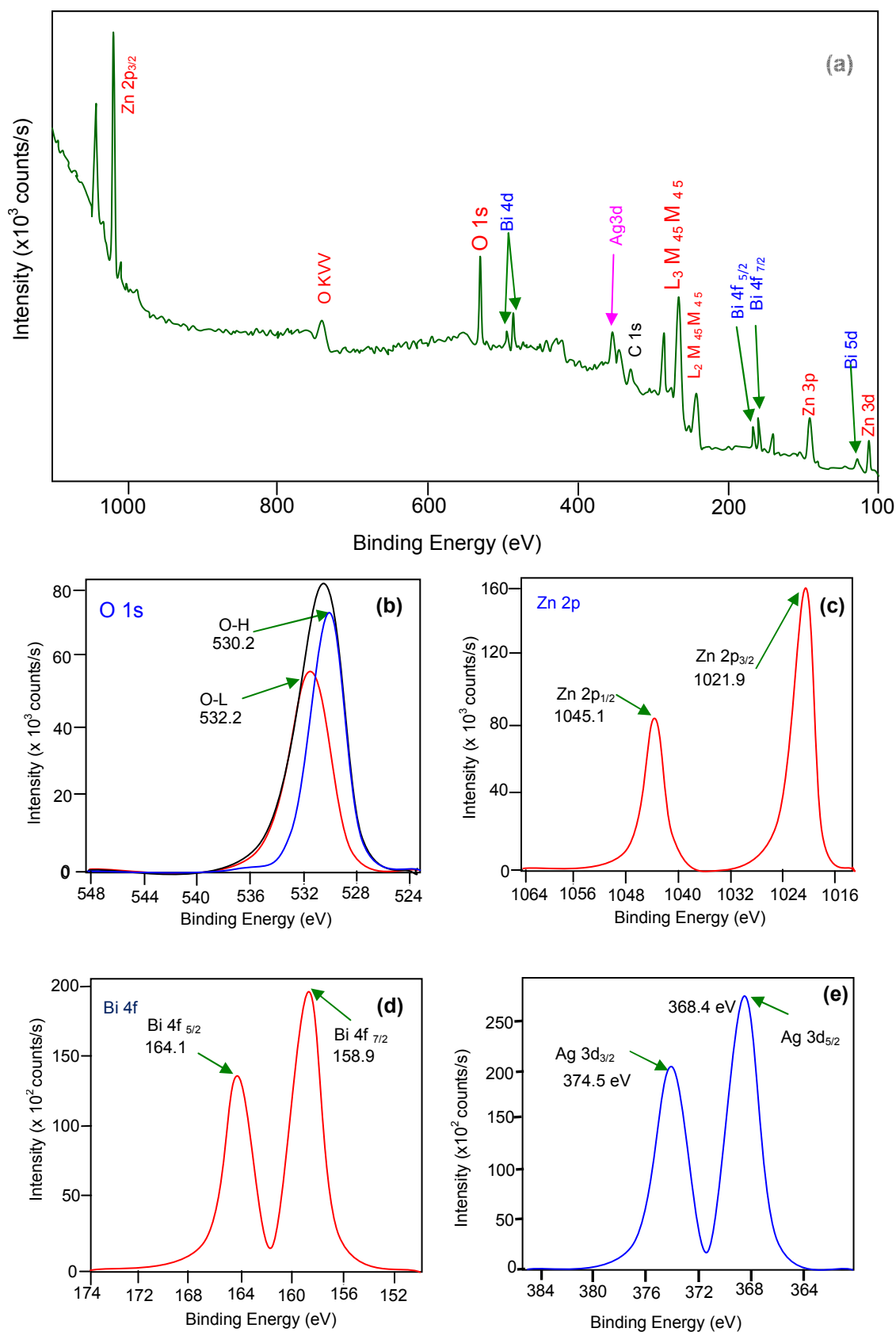


Fig. 6 XPS analysis of 9wt% Ag-Bi₂O₃-ZnO (a) Survey spectrum, (b) O 1s, (c) Zn2p, (d) Bi 4f and (e) Ag 3d.

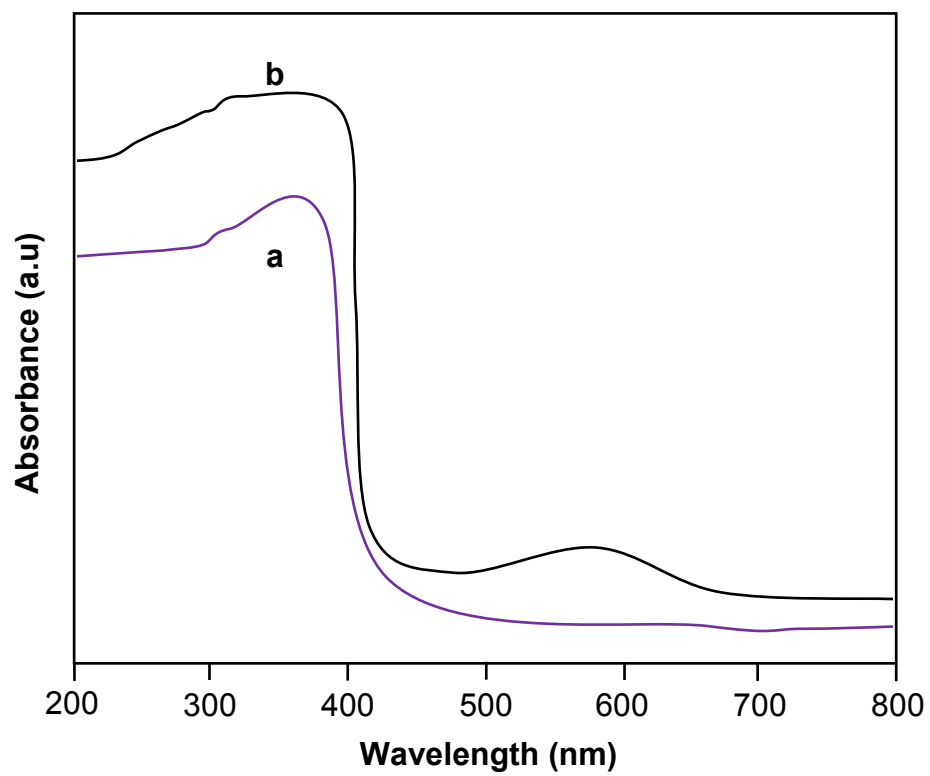


Fig. 7 Diffuse reflectance spectra (a) prepared ZnO and (b) 9wt% Ag-Bi₂O₃-ZnO.

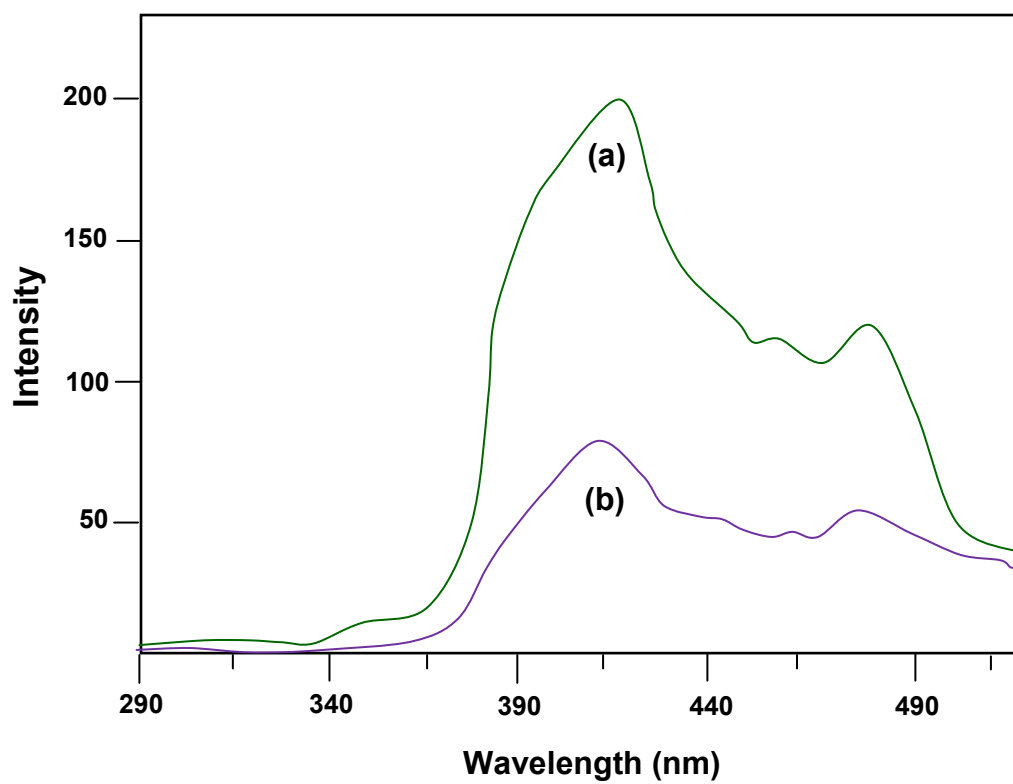


Fig. 8 Photoluminescence spectra of (a) Prepared ZnO and (b) 9wt% Ag-Bi₂O₃-ZnO.

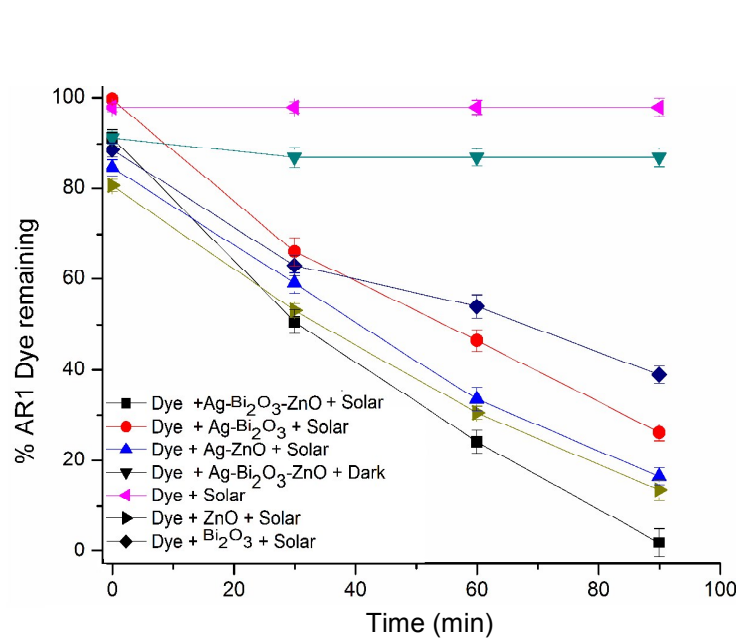


Fig. 9 Primary analysis of Ag-Bi₂O₃-ZnO: AR 1 dye concentration = 5×10^{-4} M, catalyst suspended = 4 g L^{-1} , pH = 7, airflow rate = 8.1 mL s^{-1} , $I_{solar} = 1250 \times 100 \text{ Lux} \pm 100$.

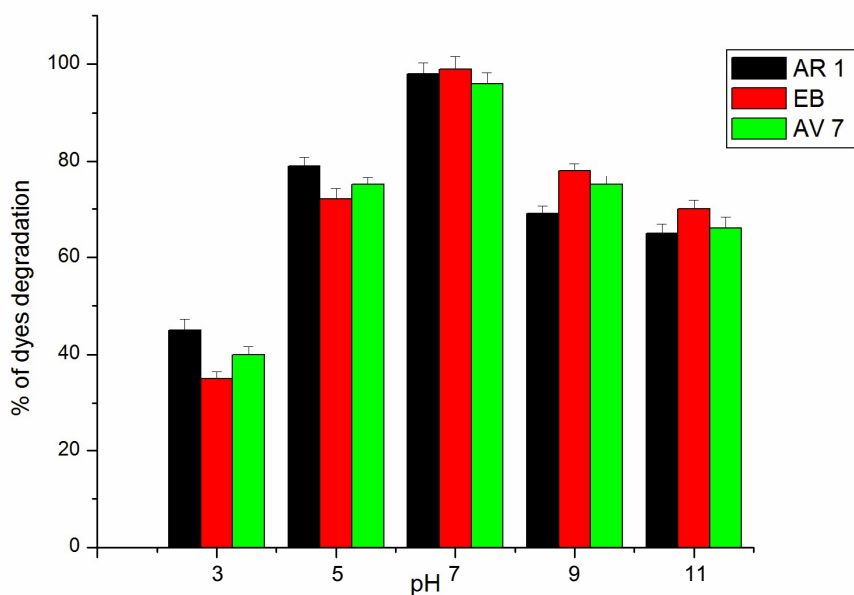


Fig. 10 Effect of solution pH; AR 1 dye concentration = 5×10^{-4} M, catalyst suspended = 4 g L^{-1} , airflow rate = 8.1 mL s^{-1} , $I_{\text{solar}} = 1250 \times 100 \text{ Lux} \pm 100$, (b) EB dye concentration = 5×10^{-4} M, catalyst suspended = 4 g L^{-1} , airflow rate = 8.1 mL s^{-1} , $I_{\text{solar}} = 1250 \times 100 \text{ Lux} \pm 100$ lx, (c) Primary analysis: AV 7 dye concentration = 5×10^{-4} M, catalyst suspended = 4 g L^{-1} , airflow rate = 8.1 mL s^{-1} , $I_{\text{solar}} = 1250 \times 100 \text{ Lux} \pm 100$.

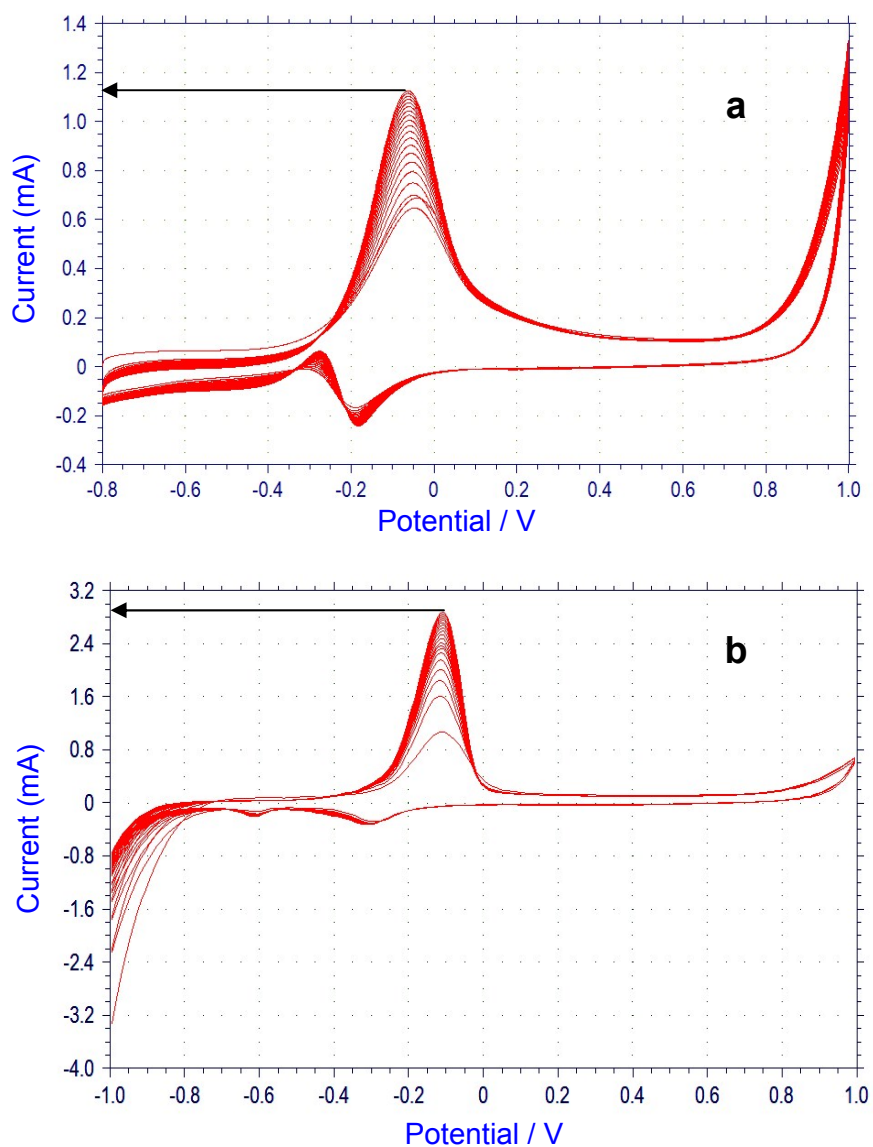
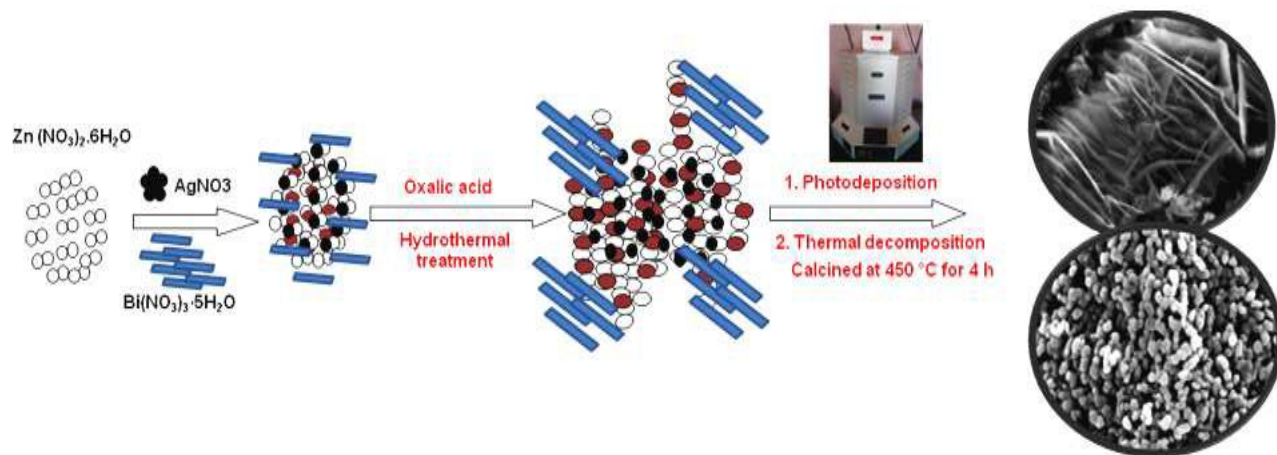
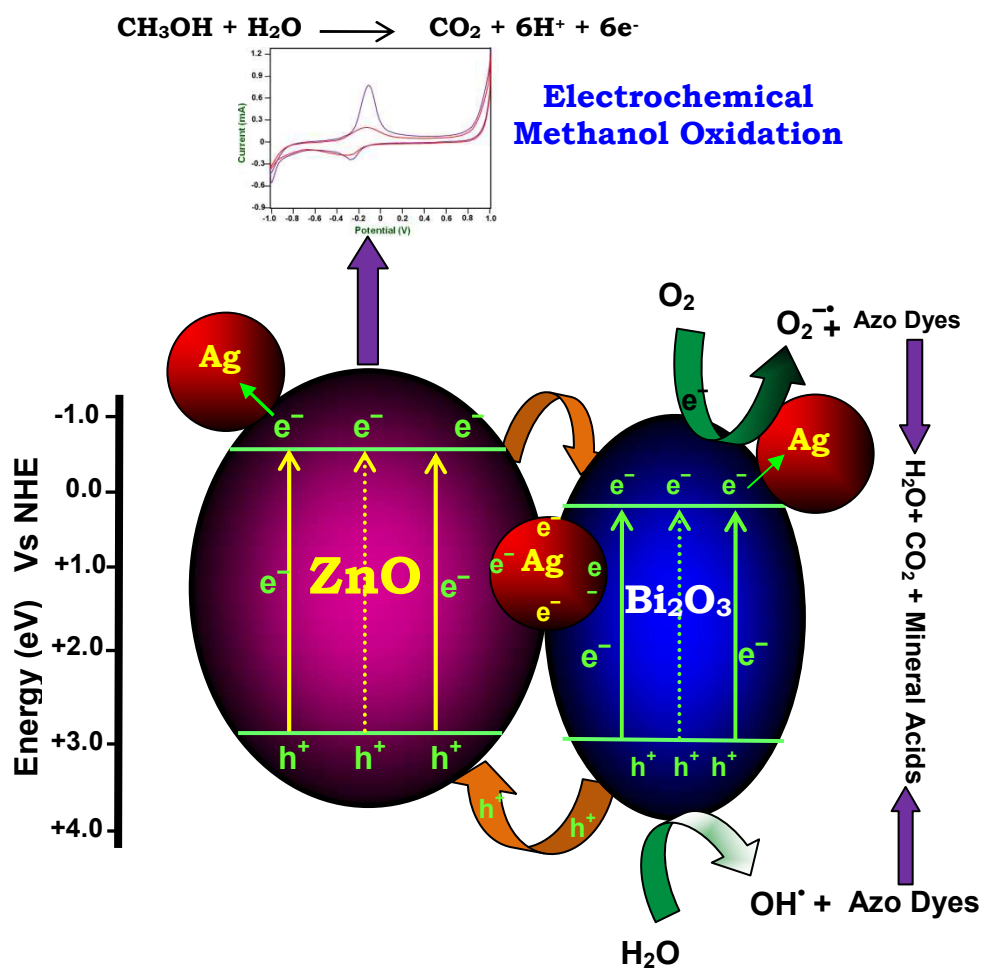


Fig. 11 Cyclic Voltammogram of (a) Prepared ZnO and (b) 9wt% Ag-Bi₂O₃-ZnO in N₂ and saturated 0.5M NaOH + 0.5 M CH₃OH solution at a scan rate of 50 mVs⁻¹ at 25 °C.

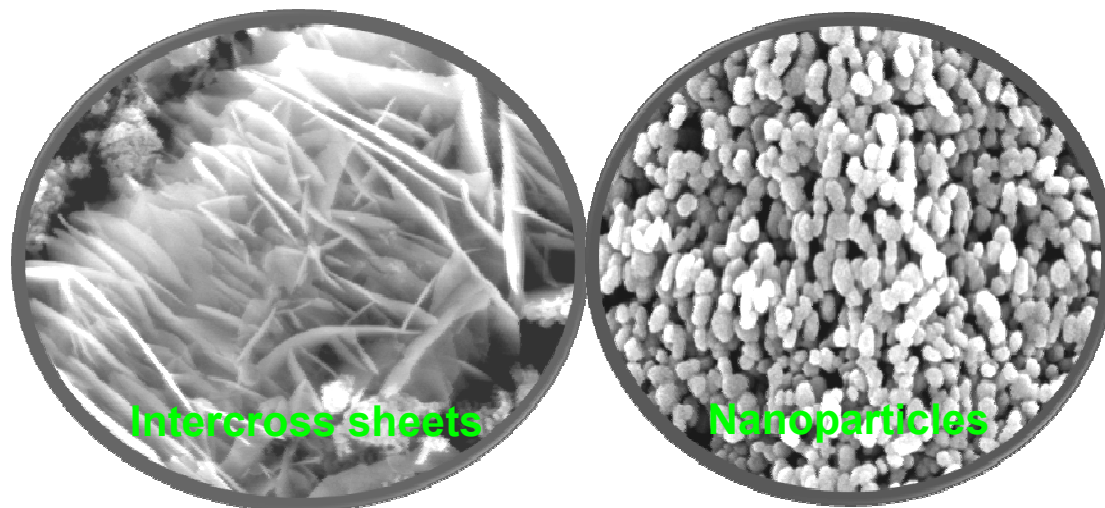


Scheme 1. Schematic representation of preparation of Ag-Bi₂O₃-ZnO



Scheme 2. Dye degradation mechanism.

TOC

Heterostructured Ag-Bi₂O₃-ZnO

Bifunctional heterostructured Ag-Bi₂O₃-ZnO was fabricated by template free photodeposition–hydrothermal method. The HR-SEM images revealed the formation of organized intercrossed sheets and peanut shell like structure, which were composed of nanosheets and nanoparticles respectively. Ag-Bi₂O₃-ZnO has enhanced absorption in the UV and visible region when compared to Bi₂O₃ and ZnO. Ag-Bi₂O₃-ZnO is stable and reusable without appreciable loss of catalytic activity up to four consecutive cycles. Ag-Bi₂O₃-ZnO shows enhanced electrochemical methanol oxidation when compared to Ag-Bi₂O₃, Bi₂O₃-ZnO, Ag-ZnO and ZnO. Enhancement in methanol oxidation current, demonstrates its high potential as anode catalyst in direct methanol fuel cells.